

Complex Self-Assembled Morphologies of Thin Films of an Asymmetric $A_3B_3C_3$ Star Polymer

Yecheol Rho,^{†,‡} Changsub Kim,^{†,‡} Tomoya Higashihara,^{†,§} Sangwoo Jin,[‡] Jungwoon Jung,[‡] Tae Joo Shin,^{||} Akira Hirao,^{*,§} and Moonhor Ree^{*,‡,||}

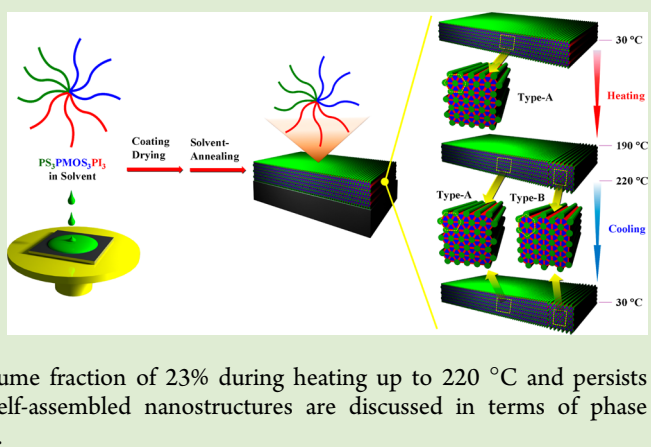
[‡]Department of Chemistry, Division of Advanced Materials Science, Center for Electro-Photo Behaviors in Advanced Molecular Systems, Polymer Research Institute, and BK School of Molecular Science, Pohang University of Science and Technology, Pohang 790-784, Republic of Korea

[§]Polymeric and Organic Materials Department, Graduate School of Science and Engineering, Tokyo Institute of Technology, H-127, 2-12-1, O-okayama, Meguro-ku, Tokyo 152-8552, Japan

^{||}Pohang Accelerator Laboratory, Pohang University of Science and Technology, Pohang 790-784, Republic of Korea

S Supporting Information

ABSTRACT: An asymmetric nine-arm star polymer, (polystyrene)₃-(poly(4-methoxystyrene))₃-(polyisoprene)₃ (PS₃-PMOS₃-PI₃) was synthesized, and the details of the structures of its thin films were successfully investigated for the first time by using in situ grazing incidence X-ray scattering (GIXS) with a synchrotron radiation source. Our quantitative GIXS analysis showed that thin films of the star polymer molecules have very complex but highly ordered and preferentially in-plane oriented hexagonal (HEX) structures consisting of truncated PS cylinders and PMOS triangular prisms in a PI matrix. This HEX structure undergoes a partial rotational transformation process at temperatures above 190 °C that produces a 30°-rotated HEX structure; this structural isomer forms with a volume fraction of 23% during heating up to 220 °C and persists during subsequent cooling. These interesting and complex self-assembled nanostructures are discussed in terms of phase separation, arm number, volume ratio, and confinement effects.



Block copolymers have attracted much attention in the field of nanotechnology over the past two decades because of their morphologies; these morphologies are particularly affected by phase separation, which depends strongly on the block components and compositions.^{1–3} The morphologies of block copolymers have also been studied extensively with regard to the interaction energies of the block components, entropy variations with molecular weight, and block volume ratios.⁴ As a result, various morphologies have been discovered and their formation mechanisms established.^{1–4} However, these studies have mostly concentrated on linear-type block copolymers because of their relatively easy syntheses.

Asymmetric star polymers have arms that differ in chemical structure and have received significant attention because of their potential to form novel morphologies that are more complex than those of linear-type polymers and block copolymers.^{5–8} Several ABC-type star polymers with three arms have been reported^{6–9} and found to exhibit complex morphological structure, including mixed structures.^{6–8} However, they have mostly been examined in the bulk state by using conventional transmission electron microscopy and X-ray scattering.^{6–8} Further, such star polymers were initially limited to three arms because of the difficulties of synthesizing polymers with a higher number of arms. Recently, a novel

iterative methodology based on living anionic polymerization with specially designed 1,1-diphenylethylene derivatives⁹ has been developed that overcomes these difficulties. Moreover, synchrotron grazing incidence X-ray scattering (GIXS) has been demonstrated to have significant advantages over conventional X-ray scattering and neutron scattering: (i) a high intensity scattering pattern is always obtained, even for films of nanoscale thickness, because the X-ray beam path length through the film plane is sufficiently long; (ii) there is no unfavorable scattering from the substrate on which the film is coated; and (iii) sample preparation is easy.¹⁰ In addition, GIXS is a nondestructive technique, in contrast to transmission electron microscopy, which is destructive. The successful syntheses of multiarm star polymers and the emergence of the powerful GIXS technique prompted us to investigate the structural details of thin films of an asymmetric multiarm star polymer.

In this study, we synthesized an asymmetric nine-arm star polymer, (polystyrene)₃-(poly(4-methoxystyrene))₃-(polyisoprene)

Received: July 11, 2013

Accepted: September 5, 2013

Published: September 13, 2013

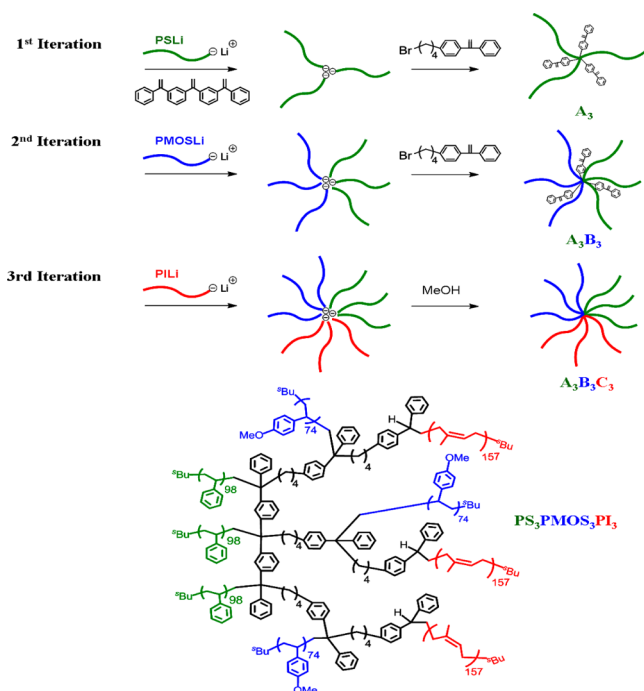


Figure 1. Synthetic route for the asymmetric nine-arm star polymer $\text{PS}_3\text{-PMOS}_3\text{-PI}_3$.

prene)₃ ($\text{PS}_3\text{-PMOS}_3\text{-PI}_3$) and investigated the phase-separated structures and orientation details of its thin films by using in situ GIXS with a synchrotron radiation source. Quantitative

GIXS analysis was successfully performed for the first time, and we found that in thin films the asymmetric nine-arm star polymer molecules undergo phase separation favorably via chloroform-annealing and, interestingly, form a well-defined hexagonal (HEX) structure composed of truncated PS cylinders and PMOS triangular prisms with a main director that is preferentially oriented in the film plane. Furthermore, this HEX structure was found to undergo a partial rotational transformation process at temperatures above 190 °C, which results in the formation of a 30°-rotated HEX structure. These interesting and complex self-assembled nanostructures are discussed here in detail in terms of phase separation, arm number, volume ratio, and confinement effects.

The nine-arm star polymer $\text{PS}_3\text{-PMOS}_3\text{-PI}_3$ was successfully synthesized (Figure 1; see the synthesis section in the Supporting Information) according to a previously reported method.⁹ The nine-arm star polymer was determined to have a number-average molecular weight \overline{M}_n of 103000 and a polydispersity index PDI of 1.04; for the PS arms, $\overline{M}_n = 10200$ and PDI = 1.02; for the PMOS arms, $\overline{M}_n = 9970$ and PDI = 1.04; for the PI arms, $\overline{M}_n = 10700$ and PDI = 1.02 (see the Supporting Information). Synchrotron X-ray reflectivity analysis found that in thin films the PS, PMOS, and PI homopolymers (with \overline{M}_n values close to those of the corresponding arms in the nine-arm star polymer) have electron densities ρ_e of 330 nm⁻³, 346 nm⁻³, and 287 nm⁻³, respectively (see Figure S1 in the Supporting Information). From these data, the mass densities of the PS, PMOS, and PI homopolymers were estimated to be 1.05, 1.09, and 0.87 g/

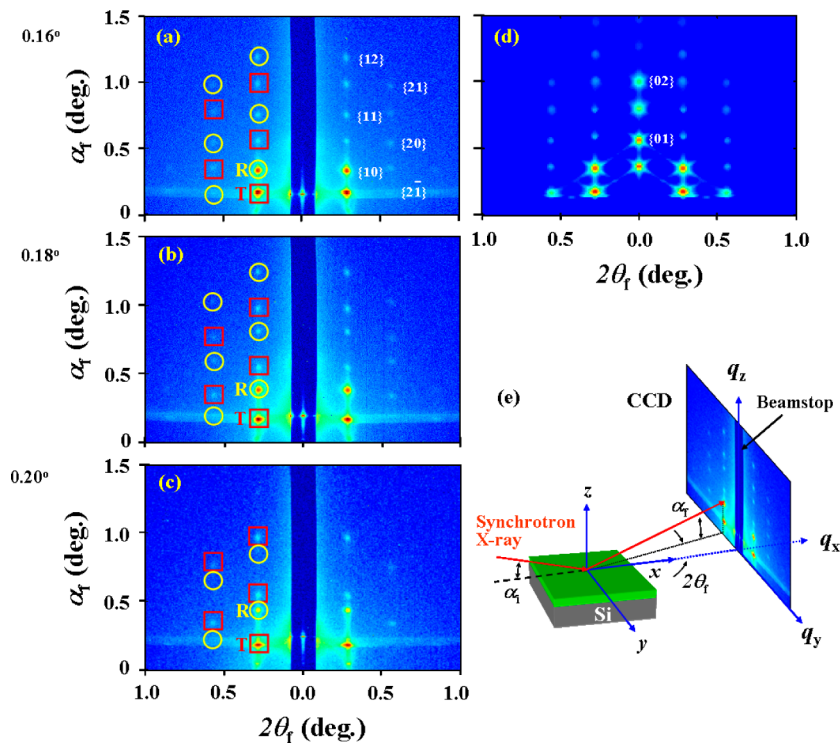


Figure 2. 2D GIXS patterns measured with various incidence angles α_i at 25 °C for CHCl_3 -annealed thin films of the $\text{PS}_3\text{-PMOS}_3\text{-PI}_3$ star polymer deposited on silicon substrates: (a) $\alpha_i = 0.160^\circ$; (b) 0.180° ; and (c) 0.200° . The letter R and the circles indicate the scattering spots generated by the reflected X-ray beam, and the T and squares indicate the scattering spots generated by the transmitted X-ray beam; some scattering spots were indexed with the results of data analysis. (d) The scattering image for $\alpha_i = 0.160^\circ$ reconstructed from the structural parameters of the HEX truncated cylinder and triangular prism structure (Table 1) by using the GIXS formula. (e) Geometry of GIXS: α_i and $2\theta_f$ are the out-of-plane and in-plane exit angles of the out-going X-ray beam, respectively, and q_x , q_y , and q_z are the components of the scattering vector q .

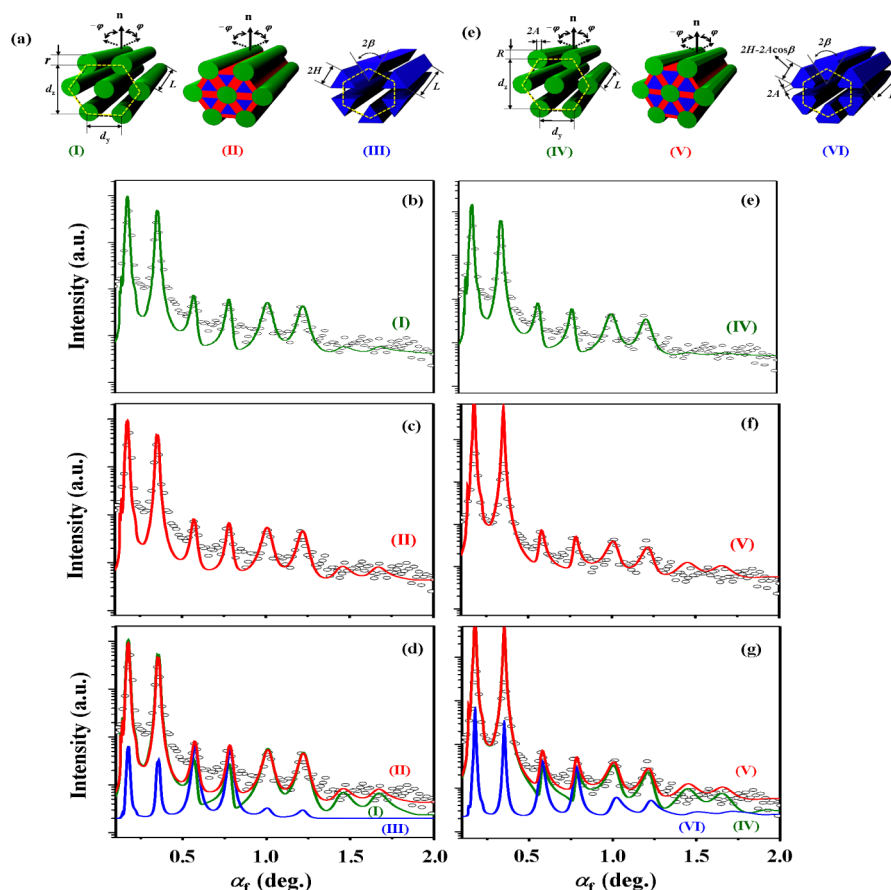


Figure 3. (a) Structural models considered for the phase-separated nanostructures in the CHCl_3 -annealed PS_3 - PMOS_3 - PI_3 thin film: (I) simple HEX cylinder structure; (II) HEX cylinder and triangle prism structure; (III) HEX triangle prism structure; (IV) HEX truncated cylinder structure; (V) HEX truncated cylinder and triangle prism structure; (VI) HEX truncated triangle prism structure. The structural parameters of these models are presented in Table 1. Out-of-plane scattering profiles were extracted along the α_f direction at $2\theta_f = 0.286^\circ$ from the 2D scattering pattern in Figure 2a and fitted with the GIXS formulas derived for the structural models in (a); (b) I; (c) II; (d) II and the contributions of its structural components (I and III); (e) IV; (f) V; (g) V and the contributions of its structural components (IV and VI). The open circles are the measured data points, and the solid lines were obtained by fitting the data according to the GIXS formulas of the chosen structural models.

cm^3 , respectively; here the mass densities of the PS and PI homopolymers are comparable to previously reported values.¹¹ Furthermore, the volume fractions of the PS, PMOS, and PI arm components in the nine-arm star polymer were estimated to be 31.4, 29.4, and 39.2%, respectively.

Synchrotron GIXS measurements (Figure 2e) were conducted on thin films (250–300 nm thick) of PS_3 - PMOS_3 - PI_3 to obtain structural information. Figure 2a shows a representative two-dimensional (2D) GIXS pattern for a nine-arm star polymer film annealed under chloroform (CHCl_3) vapor at room temperature, which was obtained with a grazing incidence angle α_i of 0.160° at 25°C . This scattering pattern contains a number of sharp scattering spots over a wide range of scattering angles. The identification of these scattering spot arrays is somewhat complicated because they are generated by both the transmitted and reflected X-ray beams and, furthermore, partially overlap. These scattering spot arrays can be sorted into scattering spots originating from the reflected X-ray beam and those originating from the transmitted X-ray beam by varying the incidence angle α_i . GIXS patterns were also obtained at the grazing incidence angles, $\alpha_i = 0.180$ and 0.200° , as shown in Figure 2b,c. By analyzing this series of GIXS measurements, the scattering spots generated by the transmitted and reflected X-ray beams were identified; the scattering spots generated by the transmitted X-ray beam are marked by

squares and the letter T, while those generated by the reflected X-ray beam are marked by circles and the letter R. In Figure 2a, spots (marked with squares) originating from the transmitted X-ray beam are present at 0.18° , 0.58° , and 1.00° along the α_f direction at $2\theta_f = 0.286^\circ$ with relative scattering vector lengths from the specular reflection position of 1, $\sqrt{3}$, and 2, respectively. Scattering spots (marked with circles) due to the reflected X-ray beam are present at 0.35° , 0.77° , and 1.20° along the α_f direction at $2\theta_f = 0.286^\circ$ with relative scattering vector lengths from the specular reflection position of 1, $\sqrt{3}$, and 2, respectively. These scattering spots show that phase-separated microdomains with a hexagonal (HEX) cylinder structure are present in the nine-arm star polymer film; the cylinders lie in the film plane.

We attempted to quantitatively analyze the scattering data with GIXS formulas derived for several HEX structure models (see the derivation details in the Supporting Information) in order to determine the structural details of the phase-separated nine-arm star polymer films. First, we considered a simple HEX cylinder structure model (Figure 3a-I). As shown in Figure 3b, the out-of-plane scattering profile can be approximately fitted with the GIXS formula derived for a simple HEX cylinder structure model. The obtained structural parameters are listed in Table 1. The cylinder phase has the following characteristics: $R = 6.9$ nm (the mean cylinder radius), $d_f = 27.6$ nm (the mean

Table 1. Structural Parameters of Thin Films of the Asymmetric Star Polymer PS₃-PMOS₃-PI₃, as Obtained with GIXS Measurements and Data Analysis

structural parameters at a given temperature	morphological structure							
	simple HEX cylinder structure	HEX cylinder and triangular prism structure	HEX truncated cylinder structure	HEX truncated cylinder and triangular prism structure				
T (°C)	25	25	25	25	145 ^e	205 ^e	30 ^f	
R^a (nm)	6.9	6.9	7.1	7.1	7.2	7.3	7.3	
σ_R^b (nm)	0.6	0.7	0.6	0.6	0.9	0.9	0.9	
$2H^c$ (nm)		14.3			16.9	17.8	18.1	
σ_H^d (nm)		1.0			1.3	1.3	1.3	
$2\beta^e$ (deg)		76.5			78.2	74.3	67.3	
$2A^f$ (nm)					4.1	4.1	4.1	
d_y^g (nm)	27.6	27.6	27.6	27.6	27.6	29.1	29.6	
d_z^h (nm)	35.8	35.8	35.8	35.8	35.8	40.5	46.9	
d_z/d_y^i	1.29	1.29	1.29	1.29	1.29	1.49	1.68	
g_1^j	0.050	0.050	0.050	0.050	0.050	0.100	0.110	
g_2^j	0.050	0.050	0.050	0.050	0.050	0.100	0.110	
g_3^j	0.050	0.050	0.050	0.050	0.050	0.100	0.110	
ϕ_A^k	1.00	1.00	1.00	1.00	1.00	1.00	0.77	
$\overline{\varphi}_A^l$ (deg)	0.00	0.00	0.00	0.00	0.00	0.00	0.00	
$\sigma_{\varphi_A}^m$ (deg)	1.80	1.80	1.80	1.80	1.80	4.89	5.95	
$O_{s,A}^n$	0.999	0.999	0.999	0.999	0.999	0.989	0.984	
ϕ_B^o	0.00	0.00	0.00	0.00	0.00	0.00	0.23	
$\overline{\varphi}_B^p$ (deg)							0.00	
$\sigma_{\varphi_B}^q$ (deg)							7.81	
$O_{s,B}^r$							0.973	
							0.980	

^aMean radius of the cylinder or truncated cylinder. ^bStandard deviation of the radius R of the cylinder or truncated cylinder from \overline{R} . ^cMean hypotenuse of the triangular prism. ^dStandard deviation of the hypotenuse $2H$ of the triangular prism from $2\overline{H}$. ^eAngle of the isosceles triangle of the prism. ^fOne side length of truncated cylinder; this side meets the truncated side of truncated triangle prism. ^gMean interdistance of the cylinder array along a direction parallel to the film plane. ^hMean interdistance of the cylinder array along a direction normal to the film plane. ⁱRatio of d_z and d_y . ^jParacrystal distortion factor. ^kVolume fraction of the type-A hexagonal structure. ^lMean polar angle between the orientation vector \mathbf{n} of the type-A HEX structure and the out-of-plane of the film. ^mStandard deviation of the polar angle φ_A from $\overline{\varphi}_A$ in the orientation of the type-A HEX cylinder structure. ⁿSecond order orientation factor of the type-A HEX structure. ^oVolume fraction of the type-B hexagonal structure. ^pMean polar angle between the orientation vector \mathbf{n} of the type-B HEX structure and the out-of-plane of the film. ^qStandard deviation of the polar angle φ_B from $\overline{\varphi}_B$ in the orientation of the type-B HEX cylinder structure. ^rSecond order orientation factor of the type-B HEX structure. ^sHeating run. ^tCooling run.

interdistance of the cylinders along the film plane), and $d_z = 35.8$ nm (the mean interdistance of the cylinders along the out-of-plane of the film). The HEX cylinder structure has the following characteristics: $\overline{\varphi}_A = 0^\circ$ (the mean polar angle between the orientation vector \mathbf{n} of the HEX structure and the out-of-plane direction of the film) with $\sigma_{\varphi_A} = 1.8^\circ$ (the standard deviation) and $O_{s,A} = 0.999$ (the second order orientation factor), which confirm that the HEX structure is oriented preferentially in the film plane.

This simple HEX cylinder structure was assumed to consist of only two phases, namely, the cylinder phase and the matrix. However, the binary blends of the PS, PMOS, and PI homopolymers were confirmed to be immiscible (see Figure S2 for the differential scanning calorimetry (DSC) analysis results). Thus, it seems likely that another phase-separated structure will form in the cylinder phase or the matrix. For the simple HEX cylinder structure, the cylinder phase was estimated to have a volume fraction of 30.3%. This volume fraction is very close to those (31.4 and 29.4%) of the PS and PMOS arms in the nine-arm star polymer, but much lower than that (39.2%) of the PI arms. These results suggest that the cylinder phase is composed of one of the three kinds of star arms and that the matrix consists of the other two kinds of arms. Furthermore, due to the HEX cylinder structure formation characteristics and the one-end connectivity of the

arms, both of the two different arm phases separated in the matrix should have an interface with the cylinder wall. To satisfy such requirements, a HEX structure composed of cylinders and triangular prisms (Figure 3a-II; Figure 3a-I,III) was tested in the scattering data analysis. The out-of-plane scattering profile is satisfactorily fitted with the GIXS formula derived for the combined HEX cylinder and triangular prism structure model (Figure 3c). The contributions of the structural components to the out-of-plane scattering profile are displayed in Figure 3d. The determined structural parameters are listed in Table 1. The triangular prisms have the characteristics $2H = 14.3$ nm (the mean hypotenuse of the triangular prism) and $2\beta = 76.5^\circ$ (the angle of the triangular prism), in addition to the structural parameters of the cylinders. Overall, the combined HEX cylinder and triangular prism structure model fits the scattering profile better than the simple HEX cylinder structure model.

In the combined HEX cylinder and prism structure, the matrix phase is in good contact with the cylinder phase as well as with the triangular prism phase. However, the cylinders are in line contact with the prisms. Such line contacts are unrealistic. Therefore, the cylinder phase and the prism phase are likely to share more interfacial area than is the case in line contact. Taking this point into account, truncated cylinder HEX structure models without and with truncated triangular prisms were considered, as shown in Figure 3e-IV,V. The out-of-plane

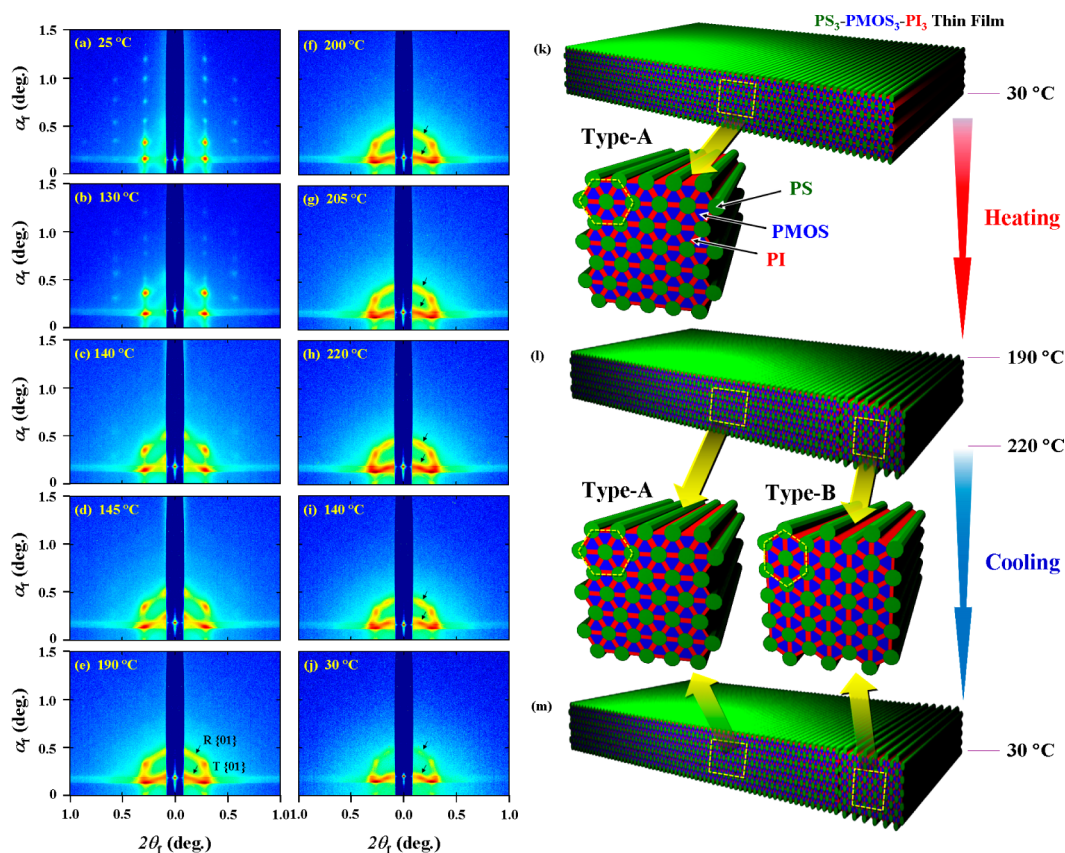


Figure 4. Representative 2D GIXS patterns of the CHCl_3 -annealed $\text{PS}_3\text{-PMOS}_3\text{-PI}_3$ thin films measured with $\alpha_i = 0.160^\circ$ during heating up to 220°C and subsequent cooling: (a–h), measured during heating; (i, j), measured during cooling from 220°C . Schematic representations of the phase-separated nanostructures in the solvent-annealed star polymer film: (k) an in-plane oriented HEX truncated PS cylinder and PMOS triangular prism structure (type-A), which is present in the range $25\text{--}190^\circ\text{C}$; (l) a mixture of the type A HEX structure and its rotational isomer (the type-B HEX structure, namely, the 30° -rotated HEX structure, which is a partially rotationally transformed type-A HEX structure) in the range $190\text{--}220^\circ\text{C}$; (m) a mixture of the type-A and -B HEX structures (here, the type-B structure was formed during the heating run) in the range $220\text{--}30^\circ\text{C}$.

scattering profile is satisfactorily fitted with the GIXS formula derived for the truncated cylinder HEX structure model (Figure 3f). This result is better than obtained with the simple HEX cylinder models without and with triangular prisms, even though truncated prisms (Figure 3-VI) were not included. Further, the scattering profile was even more satisfactorily fitted with the GIXS formula derived for the HEX truncated cylinder and triangular prism structure model (Figure 3g); the contributions of the structural components (i.e., the truncated cylinders and prisms) to the out-of-plane scattering profile are displayed in Figure 3h. Overall, the truncated cylinder and triangular prism HEX structure model produces better fitting of the scattering profile than the other HEX structure models. The determined structural parameters are listed in Table 1.

The HEX truncated cylinder and triangular prism structure is characterized by a highly preferential in-plane orientation ($O_{s,A} = 0.999$, $\overline{\varphi}_A = 0^\circ$, and $\sigma_{\varphi_A} = 1.8^\circ$) and high positional stability (i.e., a very low positional distortion factor g : $g_1 = g_2 = g_3 = 0.050$; Figure 3a-V and Table 1). The truncated (i.e., dodecagonal) cylinders were determined to have $R = 7.1$ nm (radius), $2A = 4.1$ nm (truncated side length), $d_r = 27.6$ nm, and $d_z = 35.8$ nm. The truncated triangular prisms have the following characteristics: $2H = 16.9$ nm, $2\beta = 78.2^\circ$, and $2A = 4.1$ nm. Interestingly, the d_z/d_r value is 1.29, which is smaller than that ($\sqrt{3}$) of regular HEX cylinder structures. This result shows that the HEX truncated cylinder and triangular prism structure formed in the nine-arm star polymer film is distorted

(i.e., slightly shortened) along the out-of-plane of the film and is, thus, different from a regular HEX structure. This shortening of d_z might be due to geometrical confinement effects associated with the air and substrate interface on the thin film formation process. Moreover, for the determined HEX structure, the truncated cylinders were found to have a volume fraction of 31.0%, which is very close to that (31.4%) of the PS arms in the nine-arm star polymer, and the truncated triangular prisms have a volume fraction of 29.3%, which is very close to that (29.4%) of the PMOS arms. Therefore, the truncated cylinders can be assigned to the PS arm phase, and the truncated triangular prisms can be assigned to the PMOS arm phase. Lastly, the matrix can be assigned to the PI arm phase. By using this determined structure, the scattering spots in the measured scattering patterns were assigned, as shown in Figure 2a–c. Moreover, the determined structural parameters were further used to reconstruct the 2D GIXS images. A representative of the reconstructed scattering images is displayed in Figure 2d, which is in good agreement with the experimental X-ray scattering pattern. The GIXS analysis results collectively show that the asymmetric PS, PMOS, and PI arms in the $\text{PS}_3\text{-PMOS}_3\text{-PI}_3$ thin film undergo phase separation favorably during the thin film formation process and subsequent CHCl_3 -annealing, which results in the formation of a well-defined HEX structure consisting of truncated PS cylinders and PMOS triangular prisms in the PI matrix; this

complex nanostructure is highly ordered and oriented preferentially in the film plane.

The nine-arm star polymer films were further investigated during heating up to 220 °C and subsequent cooling by using in situ GIXS analysis in order to characterize their structural stability and to identify any possible phase transitions. During the heating run, the scattering pattern varies very little in its intensity and shape at temperatures up to 135 °C; above this temperature, the scattering pattern significantly weakens in intensity but does not disappear until 220 °C (Figures 4a–h). The weakened scattering pattern at 220 °C was found to persist during subsequent cooling to room temperature (Figures 4h–j). Surprisingly, new scattering spots appear at 190 °C, in addition to the scattering reflection peaks of the HEX truncated cylinder and triangular prism structure (type-A) formed in the star polymer film (see the spots marked with arrows in Figure 4e). These new peaks increase in intensity with increases in the temperature (Figure 4e–h). The measured scattering patterns were analyzed in detail by using the GIXS formula derived above. The analysis results are summarized in Table 1.

The in situ GIXS analysis found that the scattering spots appearing at 190 °C and higher temperatures are {01} reflections originating from the 30°-rotated HEX structure (type-B), which results from the partial transformation of the type-A HEX structure (Figures 4e,k–m and Figure S3). This type-B HEX structure persists during subsequent cooling. The type-B HEX structure is formed with a volume fraction ϕ_B of 23% during the heating and subsequent cooling runs. However, the major portion of the type-A HEX structured phase is retained during this heat treatment process. These results show that the type-A HEX structure formed in the CHCl₃-annealed star polymer films is thermally stable up to near 190 °C (which is much higher than the glass transition temperatures of the asymmetric arm phases); of course, the structural parameters were found to vary somewhat with temperature in certain levels, which might be due to thermal expansion. However, the type-A HEX structured phases undergo a partial rotational transformation around 190 °C to the type-B HEX structure. Interestingly, the formed rotational structural isomer does not return to the original type-A HEX structure during the subsequent cooling process.

In summary, in situ GIXS measurements and quantitative data analysis were successfully carried out for the first time on thin films of the interesting asymmetric star polymer PS₃-PMOS₃-PI₃. This nondestructive GIXS analysis was demonstrated to be a very powerful tool for the characterization of the complex self-assembly nanostructures of the asymmetric multiarm star polymer thin films. This analysis provided structural details of the thin films that are not easily obtained with conventional techniques. The CHCl₃-annealed films were found to have a highly ordered, preferentially in-plane oriented HEX structure consisting of truncated PS cylinders and truncated PMOS triangular prisms in the PI matrix. This complex three-phased HEX structure results from the phase separations of the asymmetric arms under the extreme conditions that their one-end was linked together and the confinement in the thin film by the air and substrate interfaces. The HEX structure is thermally stable up to near 190 °C. At 190 °C and higher temperatures (up to 220 °C), the HEX structure undergoes a partial rotational transformation that produces a 30°-rotated HEX structure. The thermally induced rotational structural isomer forms in a volume fraction of 23% and is preserved during the subsequent cooling run.

■ ASSOCIATED CONTENT

📄 Supporting Information

Experimental section (materials, synthesis, and characterization, thin film preparation, GIXS measurements, XR measurements, and thermal analyses), GIXS data analysis, XR data and analysis results, DSC data, GIXS image reconstructions, and TGA data. This material is available free of charge via the Internet at <http://pubs.acs.org>.

■ AUTHOR INFORMATION

Corresponding Author

*Tel.: +82-54-279-2120 (M.R.); +81-52-841-7579 (A.H.). Fax: +82-54-279-3399 (M.R.). E-mail: ree@postech.edu (M.R.); ahirao@email.plala.or.jp (A.H.).

Author Contributions

†These authors contributed equally to this work (Y.R., C.K., T.H.).

Notes

The authors declare no competing financial interest.

■ ACKNOWLEDGMENTS

This study was supported by the National Research Foundation (NRF) of Korea (Doyak Program 2011-0028678 and Center for Electro-Photo Behaviors in Advanced Molecular Systems 2008-0061892) and the Ministry of Science, ICT and Future Planning (MSIP; World Class University Programs (R31-2008-000-10059-0) and BK21 Program). Synchrotron GIXS and XR measurements were supported by MSIP, POSCO, and POSTECH Foundation. The work at Tokyo Institute of Technology was supported by the Ministry of Education, Science, Sports, and Culture of Japan (a Grant (B: 21350060) from a Grant-in-Aid for Scientific Research) and by Denki Chemical Co. Ltd. in Japan.

■ REFERENCES

- (1) (a) Bates, F. S.; Fredrickson, G. H. *Annu. Rev. Phys. Chem.* **1990**, *41*, 525–557. (b) Park, M.; Harrison, C.; Chaikin, P. M.; Register, R. A.; Adamson, D. H. *Science* **1997**, *276*, 1401–1404. (c) Herringhaus, S.; Jacobs, K.; Mecke, K.; Bischof, J.; Fery, A.; Ibn-Elhaj, M.; Schlagowski, S. *Science* **1998**, *282*, 916–919. (d) Fasolka, M. J.; Mayes, A. M. *Annu. Rev. Mater. Res.* **2001**, *31*, 323–355. (e) Krausch, G.; Magerle, R. *Adv. Mater.* **2002**, *14*, 1579–1583. (f) Kim, J.-S.; Kim, H.-C.; Lee, B.; Ree, M. *Polymer* **2005**, *46*, 7394–7402. (g) Yoon, J.; Yang, S. Y.; Heo, K.; Lee, B.; Joo, W.; Kim, J. K.; Ree, M. *J. Appl. Crystallogr.* **2007**, *40*, 305–312. (h) Manners, I. *Angew. Chem., Int. Ed.* **2007**, *46*, 1565–1568. (i) Park, S.; Lee, D. H.; Kim, B.; Hong, S. W.; Jeong, U.; Xu, T.; Russell, T. P. *Science* **2009**, *323*, 1030–1033. (j) Kwon, W.; Rho, Y.; Kamoshida, K.; Kwon, K. H.; Jeong, Y. C.; Kim, J.; Misaka, H.; Shin, T. J.; Kim, J.; Kim, K.-W.; Jin, K. S.; Chang, T.; Kim, H.; Satoh, T.; Kakuchi, T.; Ree, M. *Adv. Funct. Mater.* **2012**, *22*, 5194–5208.
- (2) (a) Patel, S. N.; Javier, A. E.; Beers, K. M.; Pople, J. A.; Ho, V.; Segalman, R. A.; Balsara, N. P. *Nano Lett.* **2012**, *12*, 4901–4906. (b) van Zoelen, W.; Zuckermann, R. N.; Segalman, R. A. *Macromolecules* **2012**, *45*, 7072–7082. (c) Jung, J.; Park, H.-W.; Lee, J.; Huang, H.; Chang, T.; Rho, Y.; Ree, M.; Sugimori, H.; Jinnai, H. *Soft Matter* **2011**, *7*, 10424–10428. (d) Ahn, B.; Hirai, T.; Jin, S.; Rho, Y.; Kim, K.-W.; Kakimoto, M.-a.; Gopalan, P.; Hayakawa, T.; Ree, M. *Macromolecules* **2010**, *43*, 10568–10581. (e) Yoon, J.; Jung, S. Y.; Ahn, B.; Heo, K.; Jin, S.; Iyoda, T.; Yoshida, H.; Ree, M. *J. Phys. Chem. B* **2008**, *112*, 8486–8495. (f) Hirai, T.; Leolukman, M.; Jin, S.; Goseki, R.; Ishida, Y.; Kakimoto, M.-a.; Hayakawa, T.; Ree, M.; Gopalan, P. *Macromolecules* **2009**, *42*, 8835–8843. (g) Yoon, J.; Jin, S.; Ahn, B.; Rho, Y.; Hirai, T.; Maeda, R.; Hayakawa, T.; Kim, J.; Kim, K.-W.; Ree, M. *Macromolecules* **2008**, *41*, 8778–8784.

(3) (a) Heo, K.; Yoon, J.; Jin, S.; Kim, J.; Kim, K.-W.; Shin, T. J.; Chung, B.; Chang, T.; Ree, M. *J. Appl. Crystallogr.* **2008**, *41*, 281–291. (b) Jin, S.; Yoon, J.; Heo, K.; Park, H.-W.; Shin, T. J.; Chang, T.; Ree, M. *J. Appl. Crystallogr.* **2007**, *40*, 950–958. (c) Lee, B.; Park, I.; Yoon, J.; Park, S.; Kim, J.; Kim, K.-W.; Chang, T.; Ree, M. *Macromolecules* **2005**, *38*, 4311–4323. (d) Park, I.; Lee, B.; Ryu, J.; Im, K.; Yoon, J.; Ree, M.; Chang, T. *Macromolecules* **2005**, *38*, 10532–10536.

(4) (a) Leibler, L. *Macromolecules* **1980**, *13*, 1602–1617. (b) Matsen, M. W.; Schick, M. *Macromolecules* **1994**, *27*, 4014–4015. (c) Matsen, M. W.; Bates, F. S. *Macromolecules* **1996**, *29*, 1091–1098. (e) Hashimoto, T. *Macromol. Symp.* **2001**, *174*, 69–84. (d) Lodge, T. P.; Pudil, B.; Hanley, K. J. *Macromolecules* **2002**, *35*, 4707–4717.

(5) (a) Hadjichristidis, N.; Iatrou, H.; Behal, S. K.; Chludzinski, J. J.; Disko, M. M.; Garner, R. T.; Liang, K. S.; Lohse, D. J.; Milner, S. T. *Macromolecules* **1993**, *26*, 5812–5815. (b) Milner, S. T. *Macromolecules* **1994**, *27*, 2333–2335. (c) Pochan, D. J.; Gido, S. P.; Pispas, S.; Mays, J. W.; Ryan, A. J.; Fairclough, J. P. A.; Hamley, I. W.; Terrill, N. J. *Macromolecules* **1996**, *29*, 5091–5098. (d) Beyer, F. L.; Gido, S. P.; Poulos, Y.; Avgeroroulos, A.; Hadjichristidis, N. *Macromolecules* **1997**, *30*, 2373–2376. (e) Yang, L.; Hong, S.; Gido, S. P.; Velis, G.; Hadjichristidis, N. *Macromolecules* **2001**, *34*, 9069–9073.

(6) (a) Sioula, S.; Hadjichristidis, N.; Thomas, E. L. *Macromolecules* **1998**, *31*, 5272–5277. (b) Sioula, S.; Hadjichristidis, N.; Thomas, E. L. *Macromolecules* **1998**, *31*, 8429–8432. (c) Yamaguchi, K.; Takahashi, K.; Hasegawa, H.; Iatrou, H.; Hadjichristidis, N.; Kaneko, T.; Nishikawa, Y.; Jinnai, H.; Matsui, T.; Nishioka, H.; Shimizu, M.; Furukawa, H. *Macromolecules* **2003**, *36*, 6962–6966. (d) Takano, A.; Wada, S.; Sato, S.; Araki, T.; Hirahara, K.; Kazama, T.; Kawahara, S.; Isono, Y.; Ohono, A.; Tanaka, N.; Matsushita, Y. *Macromolecules* **2004**, *37*, 9941–9946. (e) Hayashida, K.; Takano, A.; Arai, S.; Shinohara, Y.; Amemiya, Y.; Matsushita, Y. *Macromolecules* **2006**, *39*, 9402–9408. (f) Hayashida, K.; Saito, N.; Arai, S.; Takano, A.; Tanaka, N.; Matsushita, Y. *Macromolecules* **2007**, *40*, 3695–3699. (g) Matsushita, Y.; Hayashida, K.; Takano, A. *Macromol. Rapid Commun.* **2010**, *31*, 1579–1587.

(7) (a) He, X.; Huang, L.; Liang, H.; Pan, C. *J. Chem. Phys.* **2002**, *116*, 10508–10513. (b) Gemma, T.; Hatano, A.; Dotera, T. *Macromolecules* **2002**, *35*, 3225–3237. (c) He, X.; Huang, L.; Liang, H.; Pan, C. *J. Chem. Phys.* **2003**, *118*, 9861–9863. (d) Huckstadt, H.; Gopfert, A.; Abetz, V. *Macromol. Chem. Phys.* **2000**, *201*, 296–307.

(8) (a) Henke, C. S.; Thomas, E. L.; Fetters, L. J. *J. Mater. Sci.* **1988**, *23*, 1685–1694. (b) Anastasiadis, S. H.; Russell, T. P.; Satija, S. K.; Majkrzak, C. F. *Phys. Rev. Lett.* **1989**, *62*, 1852–1855. (c) Mansky, P.; Chaikin, P.; Thomas, E. L. *J. Mater. Sci.* **1995**, *30*, 1987–1992. (d) Radzilowski, L. H.; Carvalho, B. L.; Thomas, E. L. *J. Polym. Sci., Part B: Polym. Phys.* **1996**, *34*, 3081–3093. (e) Green, P. F.; Limary, R. *Adv. Colloid Interface Sci.* **2001**, *94*, 53–81. (f) Lyakhova, K. S.; Horvat, A.; Zvelindovsky, A. V.; Sevink, G. J. *Langmuir* **2006**, *22*, 5848–5855.

(9) (a) Ito, S.; Goseki, R.; Ishizone, T.; Senda, S.; Hirao, A. *Macromolecules* **2013**, *46*, 819–827. (b) Goseki, R.; Ozama, Y.; Akemine, E.; Ito, S.; Ehara, S.; Hirao, A. *Polymer* **2013**, *54*, 2049–2057. (c) Ito, S.; Goseki, R.; Senda, S.; Hirao, A. *Macromolecules* **2013**, *45*, 4997–5011. (d) Hirao, A.; Inoue, K.; Higashihara, T.; Hayashi, M. *Polym. J.* **2008**, *40*, 923–941. (e) Hirao, A.; Higashihara, T.; Inoue, K. *Macromolecules* **2008**, *41*, 3579–3587. (f) Higashihara, T.; Inoue, K.; Nagura, M.; Hirao, A. *Macromol. Res.* **2006**, *14*, 287–299. (g) Hirao, A.; Kawasaki, K.; Higashihara, T. *Sci. Technol. Adv. Mater.* **2004**, *5*, 469–477. (h) Hirao, A.; Higashihara, T. *Macromolecules* **2002**, *35*, 7238–7245.

(10) (a) Rho, Y.; Ahn, B.; Yoon, J.; Ree, M. *J. Appl. Crystallogr.* **2013**, *46*, 466–475. (b) Rho, Y.; Min, J.; Yoon, J.; Ahn, B.; Jung, S.; Kim, K.; Shah, P.; Lee, J.-S.; Ree, M. *NPG Asia Mater.* **2012**, *4*, e29. (c) Busch, P.; Rauscher, M.; Smilgies, D.-M.; Posselt, D.; Papadakis, C. M. *J. Appl. Crystallogr.* **2006**, *39*, 433–442. (d) Lee, B.; Oh, W.; Yoon, J.; Hwang, Y.; Kim, J.; Landes, B. G.; Quintana, J. P.; Ree, M. *Macromolecules* **2005**, *38*, 8991–8995. (e) Lee, B.; Yoon, J.; Oh, W.; Hwang, Y.; Heo, K.; Jin, K. S.; Kim, J.; Kim, K.-W.; Ree, M. *Macromolecules* **2005**, *38*, 3395–3405. (f) Lee, B.; Oh, W.; Hwang, Y.; Park, Y.-H.; Yoon, J.; Jin, K. S.; Heo, K.; Kim, J.; Kim, K.-W.; Ree, M. *Adv. Mater.* **2005**, *17*,

696–701. (g) Lee, B.; Park, Y.-H.; Hwang, Y.-T.; Oh, W.; Yoon, J.; Ree, M. *Nat. Mater.* **2005**, *4*, 147–150. (h) Lazzari, R. *J. Appl. Crystallogr.* **2002**, *35*, 406–421.

(11) (a) Momose, A.; Fujii, A.; Kadowaki, H.; Jinnai, H. *Macromolecules* **2005**, *38*, 7197–7200. (b) Mutch, K. J.; Duijneveldt, J. S. v.; Eastoe, J.; Grillo, I.; Heenan, R. K. *Langmuir* **2008**, *24*, 3053–3060.